Stability islands in the vicinity of separatrices of near-integrable symplectic maps

Carles Simó[(1)] and Dmitri Treschev[(2)]

[1] Dept. de Matemàtica Aplicada i Anàlisi, Univ. de Barcelona,
Gran Via, 585, Barcelona 08007, Spain,
[2] V.A. Steklov Mathematical Institute, Gubkina 8, Moscow 119991, Russia.

Abstract

We discuss the problem of existence of elliptic periodic trajectories inside lobes bounded by segments of stable and unstable separatrices of a hyperbolic fixed point. We show that such trajectories generically exist in symplectic maps arbitrary close to integrable ones. Elliptic periodic trajectories as a rule, generate stability islands. The area of such an island is of the same order as the lobe area, but the quotient of areas can be very small. Numerical examples are included.

1 Introduction

It is well known that chaos in symplectic maps close to integrable ones develops essentially in the vicinity of separatrices. Pictures obtained as a result of numerical simulations show more or less homogeneous chaotic clouds around the separatrices. Figure 1 shows an example of this fact. It has been produced using the well known Chirikov separatrix map (see section 10) with parameters $a = 0.407$, $b = 1$. This separatrix map is a simple (symmetric) model to describe the dynamics close to the separatrices of general (symmetric) systems. The top left plot shows the first 10^5 iterates of the point $A = (0.01, 0.01)$ with unstable W^u $(y = 0)$ and stable W^s $(y = -\sin(2\pi x))$ manifolds superimposed. It is hard to see any possibility of island inside the lobes bounded by these manifolds even in the right plot which displays the right lobe with the iterates of A which fall inside it when the number of iterates is increased to 10^6. The location of two period 3 islands is shown. The bottom plot shows a magnification of one of the islands.

In this paper we discuss the problem of existence of elliptic periodic trajectories inside lobes bounded by segments of stable and unstable separatrices of a hyperbolic fixed point. We show that such trajectories generically exist in one-parameter families of symplectic maps arbitrary close to integrable ones. It is important to note that these trajectories are not generated by any periodic trajectories of the unperturbed map. If ε is the perturbing parameter, their period is of order $\log(1/|\varepsilon|)$ as ε tends to zero.

Let $T_\varepsilon : N \to N$ be a family of symplectic self-maps of a two-dimensional domain N, $\varepsilon \in (-\varepsilon_0, \varepsilon_0)$ is a parameter. The map T_0 is assumed to be integrable i.e., there exists a

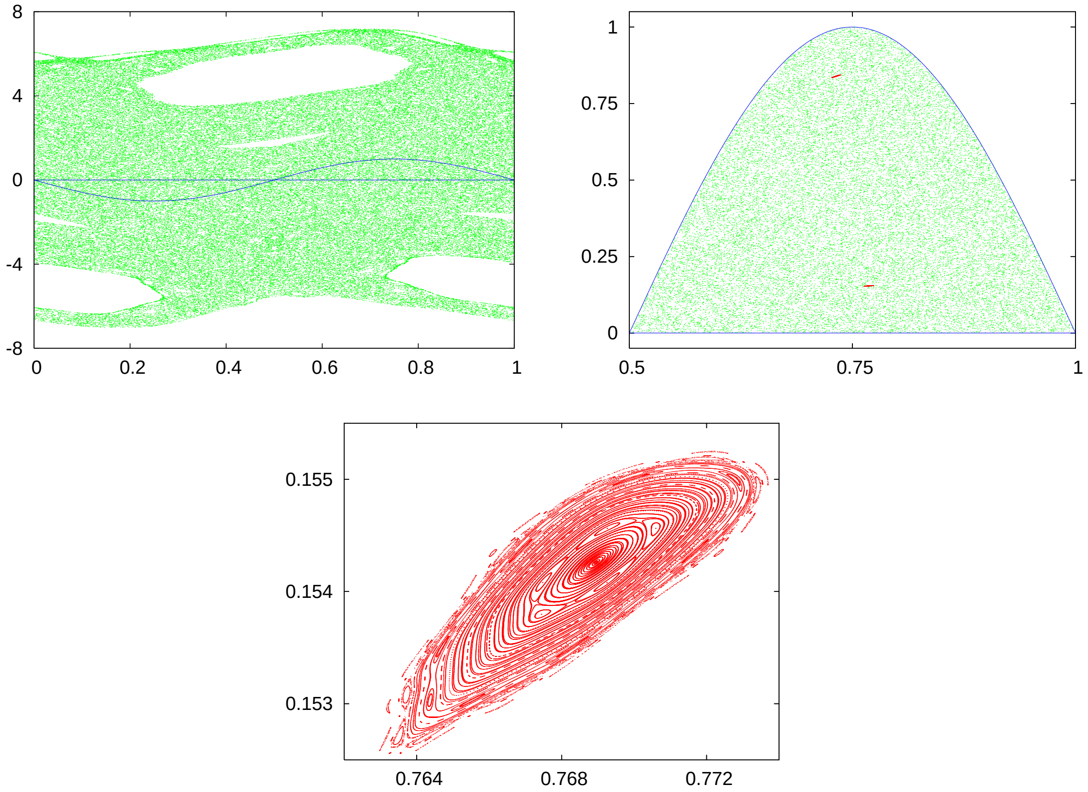

Figure 1: An example of chaotic sea covering the domain bounded by the separatrices. The Chirikov separatrix map (section 10) has been used for this illustration. Top left: a global view of a chaotic orbit. Top right: part of the same orbit inside the right lobe with two period 3 islands. Bottom: a periodic island inside the lobe. See text for details.

locally non-constant function $F : N \to \mathbb{R}$ such that $F \circ T_0 = F$. We assume that T_0 has a hyperbolic fixed point p_0, generating a figure eight separatrix curve inside N. The point p_0 is critical for the first integral F. We assume that this critical point is nondegenerate.

For small $\varepsilon \neq 0$ the map T_ε has a hyperbolic fixed point p_ε smoothly depending on the small parameter. A lot of periodic solutions near the separatrices of p_ε can be obtained by the method of symbolic dynamics, however all of them are unstable. Hence, elliptic periodic solutions should be constructed by other methods. One possible argument is as follows. When the folds of the asymptotic manifolds move and approach a tangency, new periodic solutions are created, typically by an elliptic-hyperbolic bifurcation. This gives rise to the existence of elliptic islands inside the lobe. Below we use other arguments.

Consider a Hamiltonian system with one and a half degrees of freedom depending on the parameter ε. Suppose that for $\varepsilon = 0$ the system is autonomous and has a figure-eight separatrix curve. Kozlov has shown that the condition of separatrix splitting in first approximation in ε following from the Poincaré-Melnikov theory, implies destruction of the unperturbed resonant tori situated close to the unperturbed separatrices. As a result of this destruction, nondegenerate periodic solutions appear [6]. (A multidimensional generalization of this observation is presented in [10].) All these solutions make exactly one revolution inside a separatrix loop. Some of these solutions are stable. Note that for small but fixed ε only a finite number of these solutions is guaranteed. Dovbysh [1] showed that stable periodic solutions, obtained by this method, exist only outside some $\sqrt{|\varepsilon|}$-neighborhood of the separatrices. In this context T_ε is the time-τ map, where τ is the period of the Hamiltonian with respect to time.

Sinai [9] noticed that elliptic periodic trajectories can visit lobes i.e., bi-angular domains, bounded by segments of stable and unstable separatrices, see Fig. 2. Below we call such trajectories EPL (elliptic periodic lobe) ones. An example, presented in [9], deals with a map which is far from integrable. In this paper we construct EPL-trajectories in typical nearly-integrable symplectic maps.

We associate to any periodic trajectory in a neighborhood of the separatrices its type: the number of passages near the point p_ε. In another terminology a trajectory of type n is a periodic trajectory of the corresponding separatrix map (see below) of period n.

The simplest example of EPL-trajectory is presented at Fig. 2. (Points of the trajectory are numerated in the natural way.) The trajectory revolves once inside a loop of the separatrix "eight" and goes once around the whole figure "eight". According to our classification it is of type 3. It is easy to see that there are no trajectories, visiting lobe domains, whose type is less than 3.

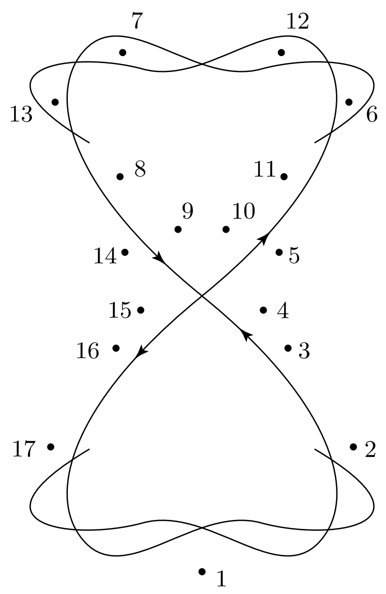

Figure 2: The simplest type of a periodic trajectory visiting lobe domains.

To formulate the results we need to specify the smoothness class of the maps we deal with. To simplify the presentation we consider the real-analytic case. However without any doubt our main results hold in C^r category, where r is sufficiently large.

Let $J = J(T_\varepsilon) \subset (-\varepsilon_0, \varepsilon_0)$ be the set of values ε, with $|\varepsilon| < \varepsilon_0$ for some fixed small ε_0, for which the map T_ε has an EPL-trajectory. (Actually, we deal only with trajectories of the type presented at Fig 2.) Suppose that the map T_0 is fixed. We put $T' = d/d\varepsilon|_{\varepsilon=0} T_\varepsilon$. Then T' is a Hamiltonian vector field.

Let T_ε be real-analytic and let $\mathcal{A}$ be the space of real-analytic vector fields on N. Below it is convenient to regard $\mathcal{A}$ as a topological space. The type of the topology is almost inessential. In particular, any topology stronger than C^2 will do.

Theorem 1 *There exists an open set $\mathcal{S} \subset \mathcal{A}$ such that for any $T' \in \mathcal{S}$, the relative measure of the set $J(T_\varepsilon)$ on the interval $(-\varepsilon_0, \varepsilon_0)$ remains greater than a positive constant, not depending on ε, when $\varepsilon_0 \to 0$.*

Conjecture. The set $\mathcal{S}$ can be chosen dense in $\mathcal{A}$.

Theorem 1 is a consequence of the corresponding result for reversible families T_ε. The reversible case can be studied easier than the general one.

Let $I_\varepsilon : N \to N$ be a real-analytic family of involutions ($I_\varepsilon^2 = \mathrm{id}$) such that $I_\varepsilon(p_\varepsilon) = p_\varepsilon$. The maps T_ε are said to be reversible with respect to I_ε (or I_ε-reversible) if

$$T_\varepsilon \circ I_\varepsilon = I_\varepsilon \circ T_\varepsilon^{-1}.$$

If T_0 is reversible, I_0 maps the separatrix "eight" onto itself. We assume that I_0 preserves loops of the "eight", i.e. it maps each of them onto itself. Such an involution acts like the symmetry in the vertical symmetry axis of the "eight".

Theorem 2 *Suppose that T_ε is reversible with respect to a family of loop-preserving involutions I_ε and at least one pair of separatrices of the point p_ε splits in the first approximation in ε. Then the relative measure of the set $J(T_\varepsilon)$ on the interval $(-\varepsilon, \varepsilon)$ exceeds some positive constant not depending on $\varepsilon \in (0, \varepsilon_0)$.*

Elliptic periodic trajectories, as a rule, generate stability islands. Below we show that the area of such an island for a generic EPL-trajectory is of the same order as the lobe area. This means that one can expect to observe these islands at pictures produced as a result of numerical simulations. However naive attempts to observe stability islands inside lobes usually fail, as illustrated in Fig. 1. There are two reasons for this. First, the measure of the set J, corresponding to "not very small" islands, is not big, despite this depends strongly on parameters of the map. If we denote by λ_0 the dominant eigenvalue of T_0 at p_0 the rough numerical estimates of section 10 for the example studied there, give that this relative measure ranges from 0.004 to 0.3 when λ_0 ranges from 1.1 to 10. Second, the averaged (with respect to ε in logarithmic scale) relative area of a "not very small" island in a lobe is usually between 10^{-8} and 10^{-4} for the same range of λ_0. Finally, the maximum (with respect to ε for ε small) of the relative area of the largest island ranges from 10^{-5} and 10^{-2}, again for the mentioned range of λ_0. See detailed information on section 10.

Because of their simplicity, periodic trajectories of type 3 could be expected to be dominant i.e., to generate the largest islands inside lobes. However, in the presence of an additional symmetry simpler trajectories can exist. Indeed, assume that any map T_ε commutes with the central symmetry $Z_\varepsilon : N \to N$, $Z_\varepsilon^2 = \mathrm{id}$ with respect to the point p_ε. Then any point $w \in N$ such that $T_\varepsilon^2(w) = Z_\varepsilon(w)$ generates a periodic trajectory of type 4. Due to the presence of the symmetry, T_ε can be regarded as a self-map of $N/\sim$, where the identification $\sim$ is performed according to Z_ε: $w' \sim z''$ iff $w' = Z_\varepsilon(w'')$. After this identification the trajectory with initial condition w turns out to have type 2 and, if it is elliptic, could be expected to be dominant. This is exactly what happens in the example displayed in section 10.

If the multiplier of the hyperbolic fixed point is very large, EPL-trajectories of higher types can also play a dominant role.

Note that a separatrix eight figure structure together with EPL-trajectories appear when a resonant invariant curve of an integrable map is destroyed by a perturbation. The main difference from the case we deal with is that in the last case the fixed point p_ε (for T_ε or some iteration of T_ε) is degenerate for $\varepsilon = 0$. This implies in particular, exponentially small separatrix splitting in the perturbed map. Theorems analogous to Theorems 1–2 hold in this case as well, but we do not present a detailed argument here. We remark, however, that in this case the relevant parameter in the corresponding separatrix map is exponentially small in ε [2]. What has been said about the smallness of the measure of J and the relative measure of the islands applies a fortiori in this case.

To prove Theorems 1–2 we perform an analysis of the maps T_ε in the vicinity of the separatrices. The main ingredient of our construction is the separatrix map. We construct it in sections 2–5. Then we use an explicit representation of the dynamics, given by the formulas of the separatrix map, for the construction of EPL orbits. Last section is devoted to numerical examples.

2 Normal coordinates

Lemma 2.1 *[7]. There exist real-analytic symplectic coordinates $(x, y) = (x(\varepsilon), y(\varepsilon))$ in a neighborhood of the hyperbolic fixed point p_ε on N such that the following assertions hold.*

(1) The coordinates of p_ε vanish.

(2) The map $T(\varepsilon)$ has the form

$$(x, y) \mapsto L_\varepsilon(x, y) = (x/\Lambda, y\Lambda), \qquad \Lambda = \Lambda(xy, \varepsilon), \tag{2.1}$$

where the function Λ is real-analytic and $\Lambda(0, \varepsilon)$ is the larger multiplier of p_ε.

On a formal level the existence of such coordinates was established by Birkhoff in C^∞ case. For real-analytic maps T_ε these coordinates were constructed by Moser, [7]. They are called normal. The map (2.1) has the first integral xy.

Remark 2.1 *The normal coordinates (x, y) are not uniquely defined. For any real-analytic at zero function $w(z)$ $(w(0) \neq 0)$ the coordinates $x' = x/w(xy)$, $y' = yw(xy)$ are normal as well.*

Remark 2.2 *Below we assume that inside the higher loop of the "eight" we have $x(\varepsilon) > 0$, $y(\varepsilon) > 0$.*

The normal coordinates $x(\varepsilon), y(\varepsilon)$ can be continued to a neighborhood of the separatrices according to the following inductive procedure. Suppose that the point $z \in N$ has the coordinates (x, y). Then we define coordinates of the points $T_\varepsilon(z)$ and $T_\varepsilon^{-1}(z)$ by $L_\varepsilon(x, y)$ and $L_\varepsilon^{-1}(x, y)$ respectively. Far from the point p_ε we have at least two different continuations of the coordinates (by T_ε^m and by T_ε^{-m}, $m \in \mathbb{N}$). Hence, we have two gluing transformations (see Fig. 3):

$$\begin{array}{lcl} U_\varepsilon^+ : \{(x, y) : x \text{ is small}, \ y > 0, y \sim 1\} & \to & \{(x, y) : x > 0, x \sim 1, \ y \text{ is small}\}, \\ U_\varepsilon^- : \{(x, y) : x \text{ is small}, \ y < 0, y \sim 1\} & \to & \{(x, y) : x < 0, x \sim 1, \ y \text{ is small}\}. \end{array} \tag{2.2}$$

The map U_ε^+ corresponds to the higher loop of the "eight" and U_ε^- to the lower one. The maps L_ε and $U_\varepsilon^\pm$ obviously commute:

$$U_\varepsilon^\pm \circ L_\varepsilon = L_\varepsilon \circ U_\varepsilon^\pm. \tag{2.3}$$

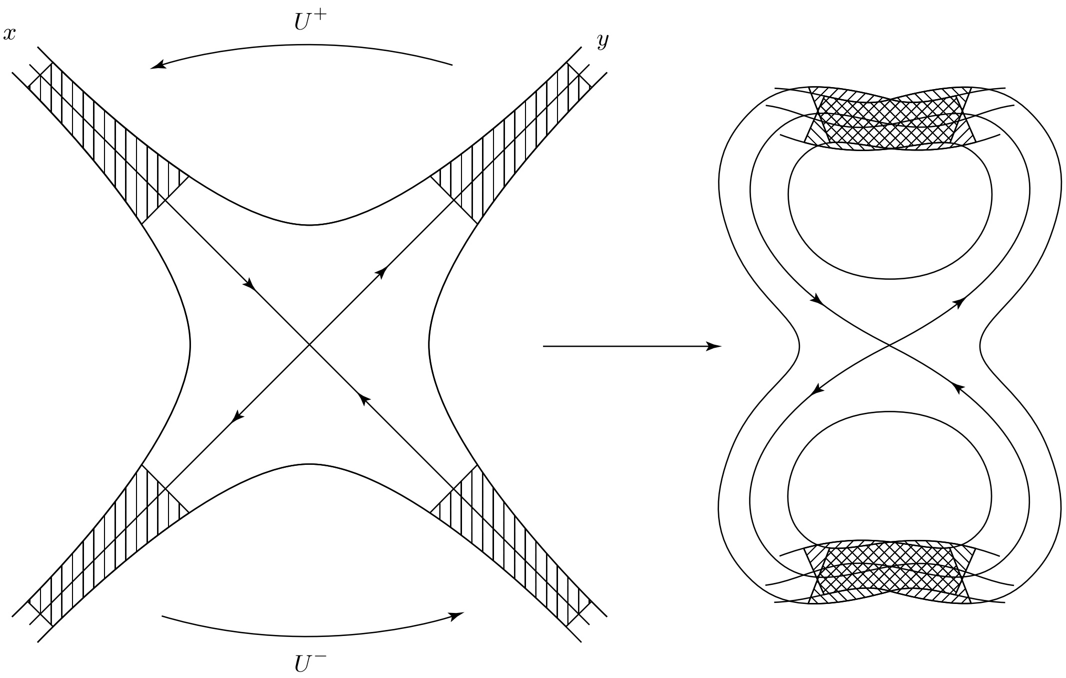

Figure 3: The (x, y)-plane and the gluing maps.

3 Gluing maps

It turns out that there is a simple formula for the maps $U_0^\pm$.

Lemma 3.1 *In the normal coordinates the first integral can be written as*

$$F = F_0 + F_1 xy + x^2y^2 f(xy), \tag{3.1}$$

where $F_1 \neq 0$ and f is a smooth function. The unperturbed gluing maps have the form

$$U_0^\pm = \big(\alpha_\pm^2 y^{-1} + O(x), \alpha_\pm^{-2} xy^2 + O(x^2)\big),$$

with positive constants $\alpha_\pm$.

Proof. Expanding the equation $F = F \circ T$ at the point $x = y = 0$, we get: $F = F_0 + F_1 xy + O(|x| + |y|)^3$, where $F_1 \neq 0$ due to the nondegeneracy of the critical point $x = y = 0$. Since F is constant on the separatrices $x = 0$ and $y = 0$, we have: $F = F_0 + F_1 xy(1 + G)$ with $G = O(|x| + |y|)$. Since xy is a first integral, G is also a first integral. This implies (3.1).

Putting $U_0^+(x, y) = (X, Y)$ we have:

$$F_0 + F_1 xy + x^2y^2 f(x, y) = F_0 + F_1 XY + X^2Y^2 f(X, Y), \quad dx \wedge dy = dX \wedge dY. \tag{3.2}$$

Recall that according to the definition of the gluing maps, X and y are bounded and separated from zero. Hence, the first equation (3.2) implies that $Y = X^{-1}(xy + O(x^2y^2))$. Substituting this to the second equation, we get:

$$x\frac{\partial X}{\partial x}(1 + O(xy)) - y\frac{\partial X}{\partial y}(1 + O(xy)) = X.$$

This implies that $X = ay^{-1}(1 + O(xy))$. It remains to show that $a > 0$. This inequality follows from our choice of normal coordinates (see (2.2)). Proposition 3.1 is proved.

The maps $U_\varepsilon^\pm$ are smooth ε-perturbations of $U_0^\pm$. Hence,

$$U_\varepsilon^\pm(x,y) = (\alpha_\pm^2 y^{-1} + O(x,\varepsilon), \alpha_\pm^{-2}xy^2 + \varepsilon y\varphi_\pm(y) + O(x^2+\varepsilon^2)). \tag{3.3}$$

The functions $\varphi_\pm$ are smooth. According to (2.3) we have:

$$\varphi_\pm(\lambda y) = \varphi_\pm(y), \qquad \lambda = \lambda(0,0). \tag{3.4}$$

Note that the function $\varphi_+(y)$ is defined for positive y while $\varphi_-(y)$ for negative ones.

4 Consequences from the reversibility

Now let us assume that the maps T_ε are I_ε-reversible, where I_ε is a smooth family of smooth loop-preserving involutions.

Lemma 4.1 *In a certain system of normal coordinates* $(\tilde{x},\tilde{y}) = (\tilde{x}(\varepsilon),\tilde{y}(\varepsilon))$ *the involutions have the form*

$$I_\varepsilon(\tilde{x},\tilde{y}) = \big(\tilde{y}(1+O(\tilde{y}\tilde{x})), \tilde{x}(1+O(\tilde{y}\tilde{x}))\big). \tag{4.1}$$

Proof. Consider the function $\Phi(x,y) = xy$. First, we show that

$$\Phi \circ I_\varepsilon = \Phi + O(\Phi^2). \tag{4.2}$$

Indeed, according to the definition of reversibility, in normal coordinates we have:

$$I_\varepsilon \circ L_\varepsilon = L_\varepsilon^{-1} \circ I_\varepsilon. \tag{4.3}$$

Since Φ is a first integral of L_ε,

$$\Phi \circ I_\varepsilon \circ L_\varepsilon = \Phi \circ L_\varepsilon^{-1} \circ I_\varepsilon = \Phi \circ I_\varepsilon.$$

Hence, $\Phi \circ I_\varepsilon$ is a first integral of L_ε. By (3.1), $\Phi \circ I_\varepsilon = c_0 + c_1\Phi + O(\Phi^2)$. Moreover, $c_0 = 0$ because $I_\varepsilon(0) = 0$. We have:

$$\Phi = \Phi \circ I_\varepsilon \circ I_\varepsilon = c_1 \Phi \circ I_\varepsilon + O(\Phi \circ I_\varepsilon)^2 = c_1^2\Phi + O(\Phi^2).$$

Therefore, $c_1 = \pm 1$. Actually, $c_1 = 1$ because I_ε is loop-preserving. This implies (4.2).

Let $I_\varepsilon^{(x)}$ and $I_\varepsilon^{(y)}$ be respectively the first and the second components of I_ε. Since I_ε exchanges stable and unstable separatrices,

$$I_\varepsilon^{(x)}(x,0) = 0, \quad I_\varepsilon^{(y)}(0,y) = 0.$$

Hence, we can put

$$I_\varepsilon^{(x)}(x,y) = ya_\varepsilon(x,y), \quad I_\varepsilon^{(y)}(x,y) = xb_\varepsilon(x,y), \tag{4.4}$$

where the functions a_ε and b_ε are smooth. By using (4.3) and (4.2), we get:

$$a_\varepsilon(x/\lambda, y\lambda) = a_\varepsilon(x,y) + O(xy), \quad b_\varepsilon(x/\lambda, y\lambda) = b_\varepsilon(x,y) + O(xy).$$

Hence,

$$a_\varepsilon(x,y) = a_\varepsilon(0,0) + O(xy), \quad b_\varepsilon(x,y) = b_\varepsilon(0,0) + O(xy).$$

According to (4.2), $a_\varepsilon(0,0)b_\varepsilon(0,0) = 1$. In particular, $a_\varepsilon(0,0)$ and $b_\varepsilon(0,0)$ do not vanish.

We have: $I_\varepsilon(x,y) = (ya_\varepsilon(x,y), x/a_\varepsilon(x,y))$. Since the involutions I_ε are loop-preserving and the coordinates (x,y) are chosen according to Remark 2.2, the inequality $a_\varepsilon(0,0) > 0$ holds. Putting $x = \tilde{x}\sqrt{a_\varepsilon(0,0)}$, $y = \tilde{y}/\sqrt{a_\varepsilon(0,0)}$ (see Remark 2.1), we obtain (4.1).

The lemma is proved.

Below we use the normal coordinates $(\tilde{x},\tilde{y})$. We skip tildes for brevity. Note that the map I_ε moves a point to another part of the "phase cross" (see Fig. 3). For example, from the "North-East" part to the "North-West" one. Below we are interested in the dynamics in an $O(\varepsilon)$-neighborhood of the separatrices. It is convenient to assume that $|x|$ is small. Hence, (x,y) lies either in the "North-East" or in the "South-West" part of the cross. The involution I_ε moves these points to other parts of the cross, but we can return their images $I_\varepsilon(x,y)$ back to the initial part of the cross, by using the inverse of the corresponding gluing map. Putting $\sigma = \operatorname{sign} y$, we obtain the following formulas:

$$(U_\varepsilon^\sigma)^{-1} \circ I_\varepsilon \begin{pmatrix} x \\ y \end{pmatrix} = \begin{pmatrix} xy^2\alpha_\sigma^{-2} - \varepsilon y\varphi_\sigma(\alpha_\sigma/y) + O(\varepsilon^2 + x^2) \\ \alpha_\sigma^2/y + O(|\varepsilon| + |x|) \end{pmatrix}. \tag{4.5}$$

Reversibility of T_ε also implies that $U_\varepsilon^\sigma \circ I_\varepsilon = I_\varepsilon \circ (U_\varepsilon^\sigma)^{-1}$. Expanding this equation in a power series in ε, we obtain an identity in zero order approximation. The first approximation yields:

$$\varphi_\sigma(y) = -\varphi_\sigma(\alpha_\sigma^2/y). \tag{4.6}$$

5 Action-angle coordinates

Dynamics of the map T_ε in the vicinity of the separatrices can be analyzed with the help of the normal coordinates x, y. Indeed, one can choose initial conditions somewhere in the "North-East" or in the "South-West" part of the cross (Fig. 3), apply the corresponding gluing map, then apply several times the hyperbolic rotation L_ε until the trajectory comes to the "North-East" or "South-West" part of the cross again, then apply a gluing map and so on. However, there exists a more convenient tool: action-angle variables:

$$p = \varepsilon^{-1}xy, \quad q = \frac{\log|y|}{\log\Lambda(xy,\varepsilon)}. \tag{5.1}$$

Since $dp \wedge dq = -(\varepsilon \log\Lambda)^{-1} dy \wedge dx$, the map T_ε in the coordinates p, q preserves the measure with density $\log\Lambda = \text{const} \cdot (1 + O(|x| + |\varepsilon|))$. Hence, for small $|\varepsilon|$ and $|x|$ the coordinates are close to symplectic ones.

The main information about the dynamics is contained in the gluing maps. In fact, the maps L_ε can be skipped completely if we consider the identification $(x,y) \sim L_\varepsilon(x,y)$. In terms of the action-angle coordinates this identification has the form $q = q \bmod 1$.

Note that since we use in (5.1) the absolute value of the variable y, we loose information about the sign of y. To restore this information we introduce the variable $\sigma = \operatorname{sign} y \in$

$\{1,-1\}$. The dynamics of T_ε in the variables p, q, σ is determined by the gluing maps. The formulas follow from (3.3) and (5.1):

$$S_\varepsilon \begin{pmatrix} p \\ q \\ \sigma \end{pmatrix} = \begin{pmatrix} P \\ Q \\ \rho \end{pmatrix} = \begin{pmatrix} p + \alpha_\sigma^2 \nu_\sigma(q - \log\alpha_\sigma/\log\lambda) + O(\varepsilon) \\ q + \frac{1+O(\varepsilon)}{\log\lambda}\Big[\log(\varepsilon\alpha_\sigma^{-2}) + \log|P|\Big] \\ \sigma \operatorname{sign} P \end{pmatrix}, \tag{5.2}$$

where

$$\nu_\sigma\Big(\frac{\log|y|}{\log\Lambda}\Big) = \varphi_\sigma(y), \qquad \sigma y > 0.$$

We call S_ε the separatrix map. According to (3.4) and (4.6) the functions $\nu_\pm$ are periodic and odd:

$$\nu_\pm(q+1) = \nu_\pm(q), \quad \nu_\pm(-q) = -\nu_\pm(q).$$

We present also formulas for the inverse separatrix map S_ε^{-1}:

$$S_\varepsilon^{-1} \begin{pmatrix} P \\ Q \\ \rho \end{pmatrix} = \begin{pmatrix} p \\ q \\ \sigma \end{pmatrix} = \begin{pmatrix} P - \alpha_\sigma^2 \nu_\sigma(q - \log\alpha_\sigma/\log\lambda) + O(\varepsilon) \\ Q - \frac{1+O(\varepsilon)}{\log\lambda}\big[\log(\varepsilon\alpha_\sigma^{-2}) + \log|P|\big] \\ \rho \operatorname{sign} P \end{pmatrix}.$$

Rewriting (4.5) in terms of the action-angle coordinates, we obtain the formulas for the involutions:

$$I_\varepsilon \begin{pmatrix} p \\ q \\ \sigma \end{pmatrix} = \begin{pmatrix} p - \alpha_\sigma^2 \nu_\sigma(-q + \log\alpha_\sigma/\log\lambda) + O(\varepsilon) \\ -q + 2\log\alpha_\sigma/\log\lambda + O(\varepsilon) \\ \sigma \end{pmatrix}. \tag{5.3}$$

6 Symmetric EPL-trajectories

To use reversibility, we search for EPL-trajectories which are symmetric in the involutions I_ε. Let the point

$$z_0 = (p_0, q_0, -1)$$

be the initial condition for such a trajectory. We assume that this point lies on the symmetry line, i.e. $I_\varepsilon(z_0) = z_0$. Then according to (5.3) we have:

$$q_0 = \log\alpha_-/\log\lambda + O(\varepsilon).$$

We write the condition of periodicity for the trajectory in the form $S_\varepsilon^{-1}(z_0) = S_\varepsilon^2(z_0)$:

$$\begin{cases} p_0 - \alpha_+^2\nu_+(-\gamma) + O(\varepsilon) = p_0 + \alpha_+^2\nu_+(\gamma) + O(\varepsilon), \\ \dfrac{\log\alpha_+}{\log\lambda} - \gamma + O(\varepsilon) \overset{\text{mod } 1}{=} \gamma + \dfrac{1}{\log\lambda}\big[\log(\alpha_+^{-1}\varepsilon) + \log|p_0 + \alpha_+^2\nu_+(\gamma)|\big] + O(\varepsilon), \\ 0 < -\operatorname{sign} p_0 = -\operatorname{sign} p_0 \operatorname{sign}(p_0 + \alpha_+^2\nu_+(\gamma)), \end{cases}$$

$$\text{being} \qquad \gamma = \frac{\log(\alpha_-^{-1}\alpha_+^{-1}\varepsilon|p_0|)}{\log\lambda}.$$

Because of the reversibility of the map, and of the symmetry of the trajectory we are looking for, the first two equations are dependent. They are equivalent to the following one:

$$1 + \lambda^{-4\kappa-m-3s-3r} = \lambda^{-2\kappa-r}\nu_+(\kappa+s+r) + O(\varepsilon), \tag{6.1}$$

where we put

$$p_0 = -\alpha_-^2 \lambda^r, \quad \varepsilon = \lambda^s, \quad \alpha_-/\alpha_+ = \lambda^\kappa \tag{6.2}$$

and the natural number m is the period of the trajectory.

7 Conditions of the stability

In this section we evaluate the trace of the monodromy matrix M, corresponding to the periodic trajectory in question. The condition of ellipticity for the trajectory has the form $|\mathrm{tr}\, M| < 2$.

The matrix M is the differential of the map S_ε^3 at the point z_0. Neglecting terms of the form $O(\varepsilon)$, we put:

$$z_1 = S_\varepsilon(z_0) = \begin{pmatrix} p_0 \\ \log(\alpha_-^{-1}\varepsilon|p_0|)/\log\lambda \\ 1 \end{pmatrix}, \tag{7.1}$$

$$z_2 = S_\varepsilon^2(z_0) = S_\varepsilon^{-1}(z_0) = \begin{pmatrix} p_0 - \alpha_+^2\nu_+\big(\log(\alpha_-\alpha_+\varepsilon^{-1}|p_0|^{-1})/\log\lambda\big) \\ \log(\alpha_-\alpha_+^2\varepsilon^{-1}|p_0|^{-1})/\log\lambda \\ 1 \end{pmatrix}. \tag{7.2}$$

The differential of the map S_ε has the form

$$DS_\varepsilon(z) = \begin{pmatrix} 1 & \alpha_\sigma^2\nu_\sigma'(q - \log\alpha_\sigma/\log\lambda)\log\lambda \\ (P\log\lambda)^{-1} & 1 + \alpha_\sigma^2\nu_\sigma'(q-\log\alpha_\sigma/\log\lambda)/P \end{pmatrix}, \tag{7.3}$$

where

$$z = (p, q, \sigma), \quad P = p + \alpha_\sigma^2\nu_\sigma\Big(q - \frac{\log\alpha_\sigma}{\log\lambda}\Big), \quad \nu_\sigma'(q) = \frac{1}{\log\lambda}\frac{d\nu_\sigma(q)}{dq}. \tag{7.4}$$

Recall that equations (7.1)–(7.4) hold with precision $O(\varepsilon)$.

The quantity $\mathrm{tr}\, M \equiv \mathrm{tr}\,\big(DS_\varepsilon(z_2)DS_\varepsilon(z_1)DS_\varepsilon(z_0)\big)$ can be reduced with the help of (7.1)–(7.3) as follows:

$$\begin{aligned} \mathrm{tr}\, M = &-2 + \lambda^{-r}\eta^{-1}\nu_-'(0)\big(1 - \lambda^{-2\kappa-r}\nu_+'(\kappa+s+r)\big) \\ &+ \big(2 - \lambda^{-r}\nu_-'(0)\big)\big(2 + \lambda^{-2\kappa-r}\eta^{-1}\nu_+'(\kappa+s+r)\big) \times \big(1 - \lambda^{-2\kappa-r}\nu_+'(\kappa+s+r)\big) + O(\varepsilon), \end{aligned} \tag{7.5}$$

where we use the notations (6.2) and

$$\eta = -1 + \lambda^{-2\kappa-r}\nu_+(\kappa+s+r) = \lambda^{-4\kappa-m-3s-3r}.$$

(The last equality follows from (6.1).)

8 EPL-trajectories exist

Suppose that the point z_0 determines the EPL-trajectory. Putting $w = s + r$, we present this assumption in the following form:

$$1 + \lambda^{-4\kappa-m-3w} = \lambda^{-2\kappa-r}\nu_+(\kappa+w) + O(\varepsilon), \tag{8.1}$$

$$\begin{aligned} \Big| &-2 + \lambda^{-r+4\kappa+m+3w}\nu_-'(0)\,\delta \\ &+ \big(2 - \lambda^{-r}\nu_-'(0)\big)\big(2 + \lambda^{2\kappa-r+m+3w}\nu_+'(\kappa+w)\big)\,\delta + O(\varepsilon)\Big| < 2, \end{aligned} \tag{8.2}$$

$$\delta = 1 - \lambda^{-2\kappa-r}\nu_+'(\kappa+w). \tag{8.3}$$

Simple properties of the system (8.1)–(8.2) are presented in the following

Proposition 8.1 *Suppose that the variables (m, r, w), $m \in \mathbf{N}$, satisfy the system (8.1)–(8.2) with the terms $O(\varepsilon)$ dropped. Then the variables $(m+3, r, w-1)$ also satisfy the same system.*

Corollary 8.1 *The set of $\varepsilon > 0$ for which there exists an EPL-trajectory, determined by (8.1)–(8.2), is asymptotically invariant under the contraction $\varepsilon \mapsto \varepsilon/\lambda$.*

Corollary 8.2 *To prove Theorem 2, it is sufficient to establish the existence of just one solution of the system (8.1)–(8.2)$|_{O(\varepsilon)=0}$.*

Corollary 8.1 is obvious. To prove Corollary 8.2 we suppose that the system (8.1)–(8.2)$|_{O(\varepsilon)=0}$ has a solution (m_0, r_0, w_0). Since the condition (8.2) is an inequality, the system (8.1)–(8.2) has, for $m = m_0$, a curvilinear interval of solutions on the plane r, w. In particular, there exists an interval $(\varepsilon_1, \varepsilon_2)$ which belongs to J. According to Corollary 8.1 the set J contains the majority (in the sense of measure) of points from the set $\cup_{n=0}^{\infty}(\lambda^{-n}\varepsilon_1, \lambda^{-n}\varepsilon_2)$. This observation implies Theorem 2.

Now we prove that there exists at least one solution of the system (8.1)–(8.2). First, note that due to the symplecticity of T_ε the average of the periodic functions $\nu_\pm$ vanishes. Since the separatrices of T_ε split in the first approximation in ε, at least one of the functions $\nu_\pm$ does not vanish identically. (In fact, $\nu_\pm$ up to a constant multiplier coincide with the Poincaré-Melnikov functions of the dynamical system T_ε, but we do not use this fact). We will suppose that $\nu_+ \not\equiv 0$, otherwise we exchange in all the previous formulas the subscripts $+$ and $-$. Since we are interested in the case of small ε, below we neglect $O(\varepsilon)$ in (8.1)–(8.2).

The argument presented below is based on the simple observation, that if the equation (8.1) holds, $\operatorname{tr} M = -2 + O(\delta)$, where (8.1)$|_{\varepsilon=0}$ implies that

$$\delta = 1 - \left(1 + \lambda^{-4\kappa - m_0 - 3w_0}\right) \frac{\nu_+'(\kappa + w_0)}{\nu_+(\kappa + w_0)}. \tag{8.4}$$

Proposition 8.2 *For any $\delta < 1$ (8.4), considered as an equation w.r.t. w_0, has a solution $w_0 \in [-1, 1]$.*

Proof of Proposition 8.2. Let $w_2 \in [0, 1]$ be a point of absolute maximum of the function $\nu_+(\kappa+w)$ and $w_1 < w_2$ the closest (from the left) to w_2 solution of the equation $\nu_+(\kappa+w) = 0$. By periodicity $w_1 > -1$. The function

$$\Psi(w) = \nu_+'(\kappa + w)/\nu_+(\kappa + w)$$

is continuous on the interval $(w_1, w_2]$. Moreover,

$$\Psi(w_1 + 0) = +\infty, \quad \Psi(w_2) = 0.$$

Hence, on the interval (w_1, w_2) there exists a point such that (8.4) holds.

Proposition 8.3 *Suppose that $m = m_0$ is large and $\delta > 0$ is small. Let $w = w_0(m_0, \delta) \in [-1, 1]$ be a solution of (8.4) and let $r = r_0(m_0, w_0, \delta)$ be a solution of (8.1). Then (m_0, r_0, w_0) satisfy (8.1)–(8.2).*

Proof of Proposition 8.3. By using (8.1) and (8.3) we get:

$$\lambda^{-2\kappa-r_0} = 1/\nu_+(\kappa+w_0) + O(\lambda^{-m_0}),$$
$$1 - \lambda^{-2\kappa-r_0}\nu'_+(\kappa+w_0) = \delta.$$

Substituting these equations into (8.2), we obtain a simpler inequality:

$$\Big| -2 + \frac{\lambda^{4\kappa+m_0+3w_0}\delta}{\nu_+(\kappa+w)}\Big[\lambda^{2\kappa}\nu'_-(0) + \big(2-\lambda^{2\kappa}\nu'_-(0)\big)\frac{\nu'_+(\kappa+w)}{\nu_+(\kappa+w)} + O(\lambda^{-m_0})\Big]\Big| < 2. \qquad (8.5)$$

Since by (8.4)

$$1 - \nu'_+(\kappa+w)/\nu_+(\kappa+w) = O(\lambda^{-m_0}) + O(\delta),$$

inequality (8.5) can be presented in the form

$$\Big| -2 + \frac{\lambda^{4\kappa+m_0+3w_0}\delta}{\nu_+(\kappa+w)}\Big(2 + O(\lambda^{-m_0}) + O(\delta)\Big)\Big| < 2.$$

This inequality holds for sufficiently small δ. Proposition 8.3 (as well as Theorem 2) is proved.

Proof of Theorem 1. Let the family T_ε be reversible with respect to a loop-preserving involution. Consider a family of symplectic maps $\hat T_\varepsilon$ such that

$$T_0 = \hat T_0, \quad \Big| d/d\varepsilon|_{\varepsilon=0} T_\varepsilon - d/d\varepsilon|_{\varepsilon=0}\hat T_\varepsilon \Big| = \Delta$$

with some small positive Δ. The separatrix map corresponding to $\hat T_\varepsilon$ also has the form (5.2), but the periodic functions $\hat\nu_\pm$, playing the role of the functions $\nu_\pm$, are not odd in general. However, they are close to the odd functions $\nu_\pm$:

$$|\hat\nu_+ - \nu_+| \sim \Delta, \quad |\hat\nu_- - \nu_-| \sim \Delta.$$

If Δ is small, an EPL-trajectory of T_ε can be continued to an EPL-trajectory of $\hat T_\varepsilon$. Since the set J for the maps T_ε consists of intervals, there exists an interval $(\hat\varepsilon_1, \hat\varepsilon_2)$ such that for any $\varepsilon \in (\hat\varepsilon_1, \hat\varepsilon_2)$ the map $\hat T_\varepsilon$ has an EPL-trajectory. Now Theorem 1 follows from the following simple assertion.

Suppose that a map T_ε with some small fixed ε has an EPL-trajectory. Then the map $T_{\varepsilon/\lambda}$ also has an EPL-trajectory (of larger period).

This assertion is a direct consequence of equations (5.2). It is an analog of Corollary 8.1.

9 Area of a stability island

The area of a stability island around an EPL-trajectory has the same order as the area of a lobe because in the action-angle coordinates both are of order one. For a given ε the area of an island around an EPL is finite and, essentially, the relative area of this island with respect to the lobe area is independent of ε.

10 Numerical examples

One of the most popular separatrix maps is the so-called Chirikov separatrix map, given by

$$(x, y) \mapsto SM_{a,b}(x, y) = (X, Y) = (x + a + b \log |Y|, y + \sin(2\pi x)), \tag{10.1}$$

where x is taken mod 1. It can be obtained from (5.2) by assuming that the upper and lower part of the figure "eight" have identical behaviour (and, hence, we disregard the sign σ) and the following choices and scalings are done, beyond neglecting the $O(\varepsilon)$ terms:

$$q = x + \frac{\log(\alpha)}{\log(\lambda)}, \quad \nu(x) = \psi \sin(2\pi x), \quad p = \alpha^2 \psi y, \quad a = \frac{\log(\varepsilon\psi)}{\log(\lambda)}, \quad b = \frac{1}{\log(\lambda)}. \tag{10.2}$$

The map (10.1) has the obvious symmetry $(x, y) \mapsto (x + 1/2, -y)$. In the scalings (10.2) the choice of the splitting function ν contains the factor ψ, to be considered as a measure of the splitting. In the case of maps ε-close to the identity the upper bound given in [2] shows that ψ is at most exponentially small in ε. As proved in different papers, like [3, 4] for some maps, and numerical evidences in many examples (see, e.g., [5] and references therein) ψ is exactly exponentially small in ε with asymptotic behaviour as predicted by the upper bound.

Concerning the "shape" of ν, the arguments in [2] show that to contain only the first harmonic must be the generic situation for maps ε-close to the identity. Degenerate examples in families having additional parameters can be found in [5].

For constant size of the splitting ψ the role of a is identical (except by a shift) to the role of s as introduced in (6.2) and, therefore, it can be assumed $a \in [0, 1)$.

An important feature of (10.1) is that the "width" of the splitting function only appears in the shift parameter a. Hence, the size of the lobe remains constant. For large b the chaotic zone reaches values up to $|y| \approx 2\pi b$, where invariant curves are found.

The stable and unstable manifolds correspond to $y = 0$ and $y = -\sin(2\pi x)$, respectively. It is clear from the symmetry that it is enough to study one of the lobes. We have chosen the upper one: $x \in [1/2, 1]$.

The numerical study of (10.1) has mainly focused on the measure of the set of a for which EPL have been detected for different values of b, on the average (with respect to a) of the fraction of the loop area covered by islands as a function of b and on the maximal (again with respect to a) size of the islands as a function of b.

To this end we have used values of b to cover a wide range of λ. Using $\mu = \log(\log(\lambda))$ the range of values of μ has been $[-4, 4]$ with step size 0.1. For each value of μ (and, hence, of λ or b) the values of a have been set to $k \times 10^{-4}$, $k = 0, \ldots, 9999$.

For each value of a, b we have used a grid of pixels with step $1/(2N)$ in x and $1/N$ in y. The lobe is covered by, roughly, $2N^2/\pi$ pixels. Typical computations have been done with $N = 2000$, some checks with $N = 4000$, reaching $N = 20000$ for a few tests. For $\mu > -2$ there is no visible difference in the plots of Fig. 4 using either $N = 2000$ or $N = 4000$.

The process to detect islands is as follows:

a) First some points close to homoclinic are iterated. Most of them have a chaotic orbit, as checked by computing the Lyapunov exponent. If points of a chaotic orbit are close to the center of one of the pixels, the pixel is marked as chaotic. The number of iterates is optimized to satisfy some accuracy in the estimate of the Lyapunov exponents and to minimize the total computational effort.

b) The pixels not marked as chaotic are examined individually. A rough Lyapunov indicator is used, with a reduced number of iterates. If the orbit is suspected to be chaotic only the initial pixel is marked as having such a character.

c) The subsisting (non marked) pixels are considered as belonging to an island. The size of the island is determined by looking at the connected components of the set of subsisting points. This can produce overestimates if some islands are too close. The period is obtained by looking at the first return of a point of an island to the same connected component.

Figure 4 displays a summary of results. The areas of the islands are given as a fraction of the area of the lobe. For $\mu < -3$ one cannot be confident on the statistics, because of the too small size of the islands. For $\mu > -2$ the top plots and the left bottom plot are quite regular, with the exception of $\mu = 1$, due to the exceptional presence of large period 6 islands, to be discussed later.

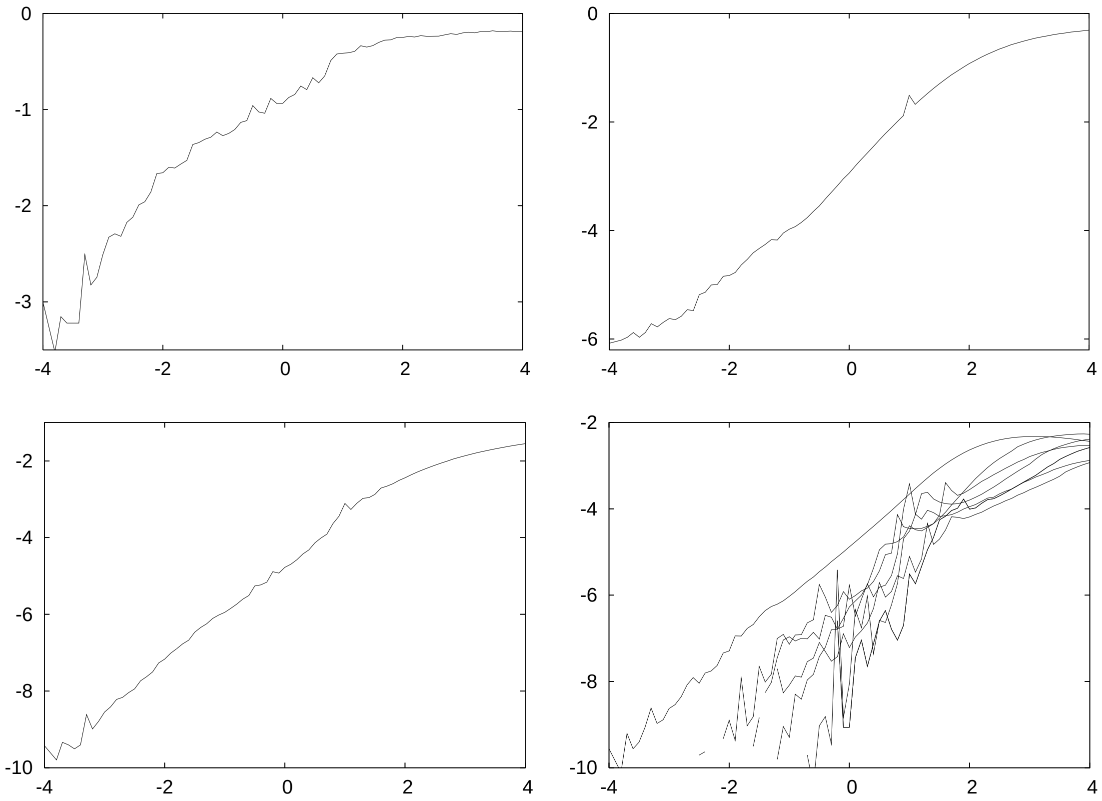

Figure 4: Statistics of results as a function of $\mu = \log(\log(\lambda))$. In all the plots the vertical variable is shown in $\log_{10}$ scale. Top left: measure of the set of a for which an island has been found. It corresponds to the value of J in Theorem 1. Top right: maximal (with respect to a) area of an island. Bottom left: average (with respect to a) total area of the islands found. Bottom right: same as the previous plot, but the contribution of different periods is displayed in different curves. The periods can be identified by the value at $\mu = 4$, which from up to down are $3, 5, 2, 4, 7, 6, 8$, respectively. The largest islands correspond to period 2, with an exception for $\mu = 1$ which has larger period 6 islands.

Figure 5 gives details of the total measure of the islands (or distribution function) for different values of μ as a function of a. By increasing μ (i.e., increasing λ or decreasing b) both the number of "visible" intervals of a for which islands exist and the maximal and average size of the islands, increase. The set of intervals has a strong structure and several scaling laws are visible. The island shown in Fig. 1, which corresponds to $\mu = 0$, $a = 0.407$, belongs to a small peak which can be seen in the top middle plot.

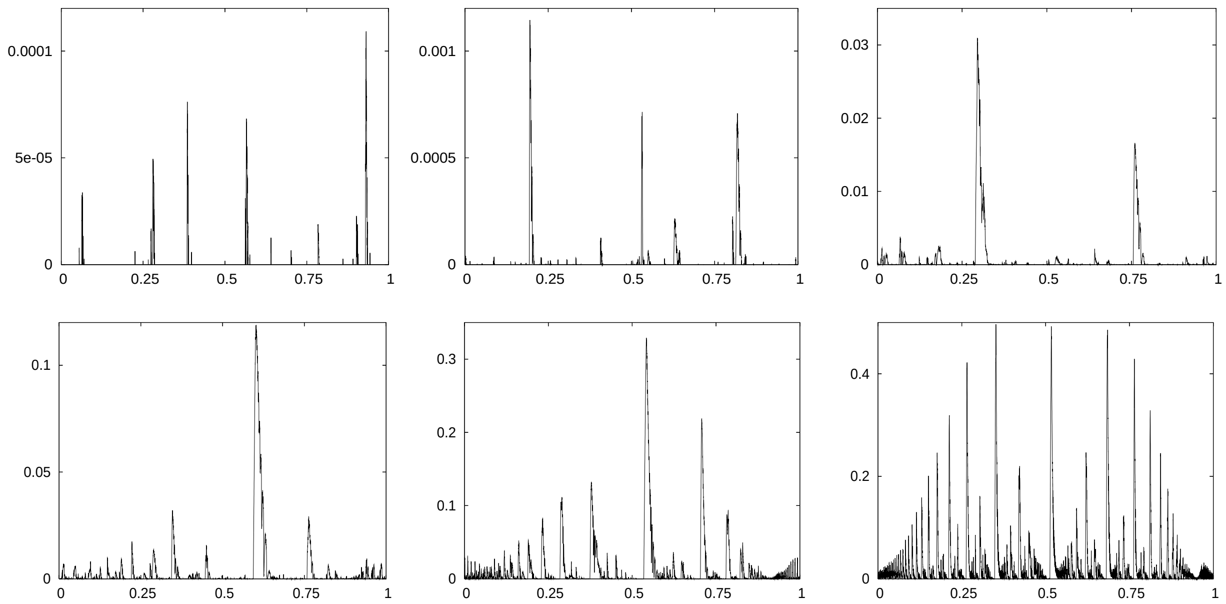

Figure 5: Measure of the totality of islands found as a function of a for different values of μ. Top: from left to right $\mu = -1, 0, 1$. Bottom: from left to right $\mu = 2, 3, 4$.

Another interesting topic is the shape of the different "peaks" seen in Fig. 5. In principle several islands of different size and period can coexist. Of course, the real number of islands can be very large, but we are talking about "visible" islands, with a size of at least one pixel. For large values of μ in the searched range up to 24 chains of islands of different period have been seen simultaneously. This affects the shape of this distribution function. Figure 6 shows a few examples for $\mu = 1, 2$. For comparison purposes we also include the area of the non-escaping points in the Hénon map as a function of $1 - \mathrm{tr}/2$, being tr the trace at the fixed point, taken from [8]. In this reference the main mechanisms to explain the features of the plot are described. In particular it is easy to see the effect of the main resonances, specially the 3:1 and 4:1 ones. One can check that the shape of the area as a function of a in the bottom left plot is almost identical to the Hénon case, specially from the middle to the right of each plot.

On the other hand the upper plots in Fig. 6 have a different shape. If in the left plot this can be due to the coexistence of several independent chains of island, the case of the right plot is different. Let us explain the origin of this difference.

Periodic islands of period k are generically created by an elliptic-hyperbolic bifurcation. It appears when a Bogdanov-Takens point occurs in the parameter space. The fixed point of $SM_{a,b}^k$ has 1 as double eigenvalue of $D\,SM_{a,b}^k$ but, as it is generic, the differential is not the identity. However, due to the symmetries of $SM_{a,b}$ it can happen that non-generic bifurcations occur. Assume that for some parameters (a, b) the differential $D\,SM_{a,b}^k$ equals the identity. For nearby parameters $(a + \Delta a, b)$ the map, in local coordinates, can be of the form

$$(\xi, \eta) \to (\bar{\xi}, \bar{\eta}) = (\gamma \Delta a + a_{20}\xi^2 + 2a_{11}\xi\eta + a_{02}\eta^2, -2a_{20}\xi\eta - a_{11}\eta^2) + O(\xi\Delta a, |(\xi, \eta)|^3).$$

If the quadratic form $a_{20}\xi^2 + 2a_{11}\xi\eta + a_{02}\eta^2$ is negative definite and $\gamma > 0$ then, for positive Δa the bifurcation gives rise to two elliptic and two hyperbolic fixed points. A reduced local model of the map is the time-1 flow of the Hamiltonian $H_{\Delta a} = (\Delta a - \xi^2 - \eta^2)\xi$.

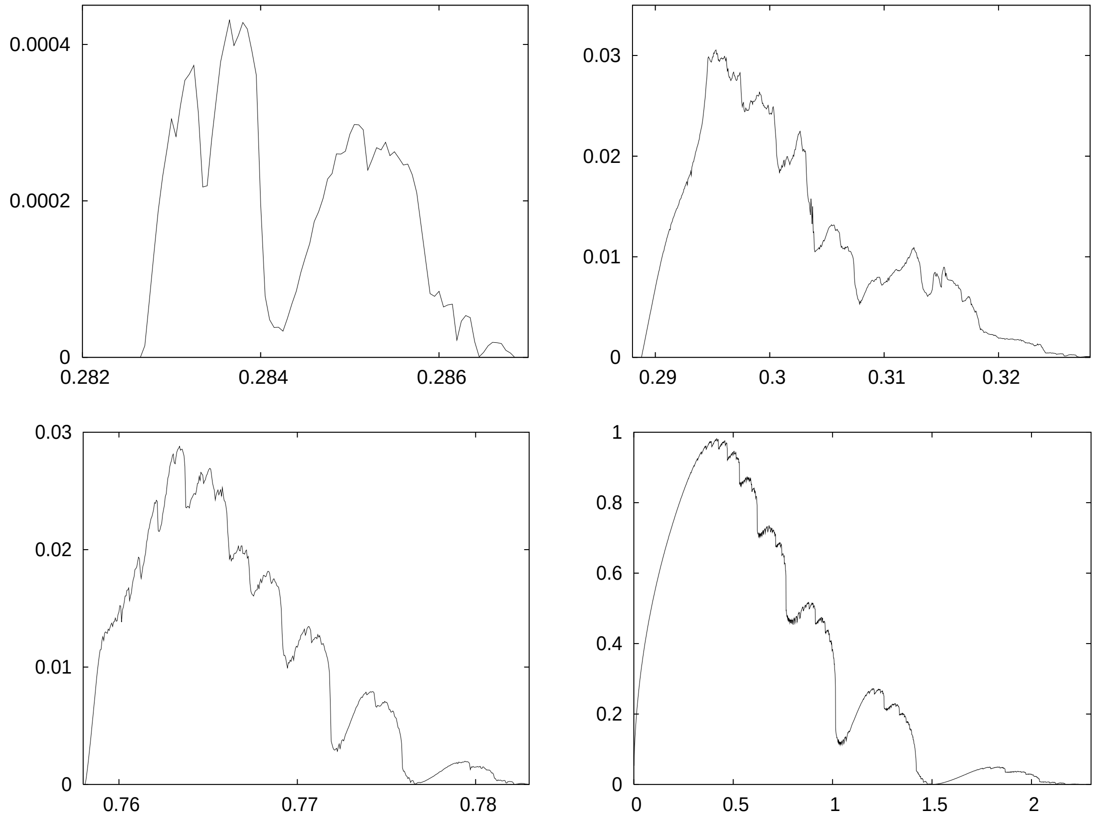

Figure 6: Measure of invariant islands as a function of a. Top: $\mu = 1$. Left: mainly corresponds to a period 3 island, but other islands of different periods $(7, 8, 12, 13, 14, 15, \ldots)$ also show up. Right: Mainly a period 6 island, with small contributions of higher periods. Bottom left: $\mu = 2$ with main contribution of a period 3 island and additional islands, specially near the left end. On the bottom right part the non-escaping area of the Hénon map (with a suitable normalization) is displayed as a function of $1 - \text{tr}/2$, where tr denotes the trace at the fixed point.

This is precisely what happens for $\mu = 1$ for the range of a shown in the top right plot of Fig. 6. As an illustration Fig. 7 displays the two period 6 islands observed for $a = 0.3$. This non-generic behaviour is also the responsible of the exceptional results which can be seen in Fig. 4 for $\mu = 1$.

For larger values of μ the same non-generic bifurcations give rise to very large islands. As an example Fig. 8 shows some examples for $\mu = 4$. For completeness not only the islands are displayed for some values of a, but also the chaotic zone, which can be seen as a "negative" of the islands, with the exception of the top right plot, due to the very narrow chaotic zone between the two periodic islands, whose width is close to 0.005 and has plenty of very small islands. We also observe that for this large value $\mu = 4$ ($b = \exp(-4)$) the chaotic zone is relatively small.

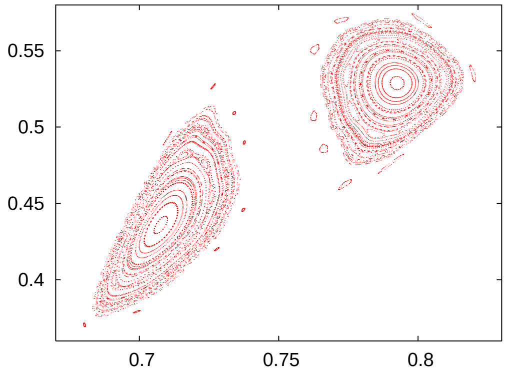

Figure 7: Two period 6 islands for $\mu = 1$ ($b = \exp(-1)$) and $a = 0.3$. The islands are obtained by evolution from the ones created by a non-generic bifurcation which appears at $(x, y) = (3/4, 1/2)$.

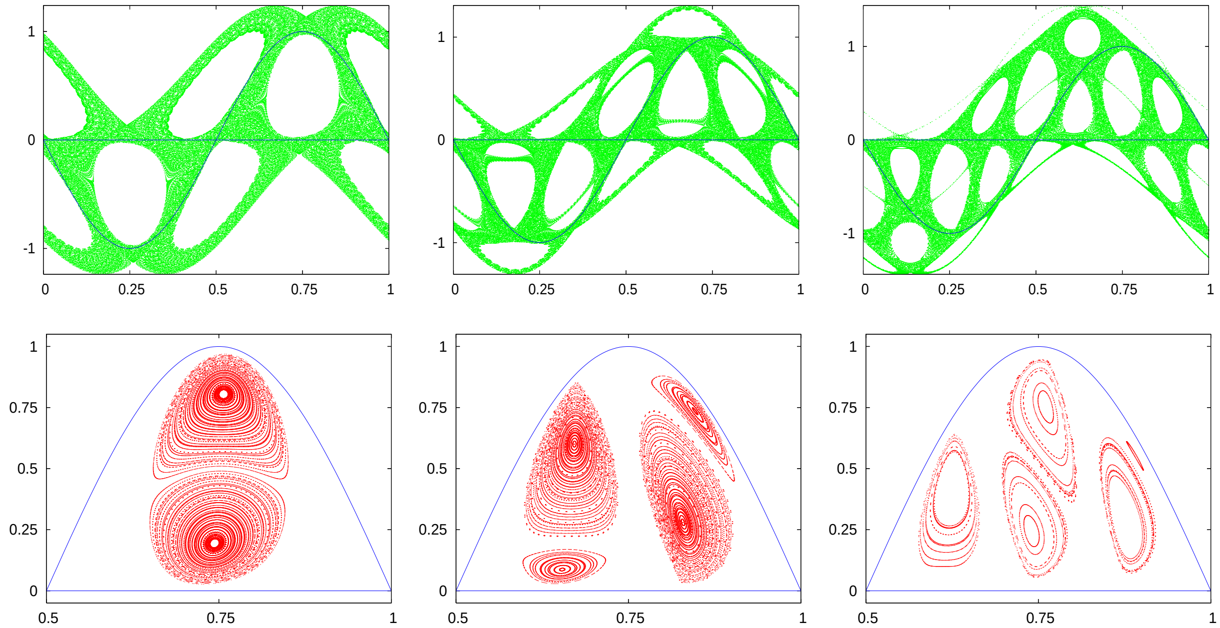

Figure 8: Large islands for $\mu = 4$. From left to right $a = 0.517, 0.352, 0.2656$. The top plots show the next 10^5 iterates of the orbit of $(0.01, 0.01)$ after a transient of 10^6 iterates. They give a good approximation of the chaotic zone. The bottom plots show, respectively, two period 2 islands, four period 3 islands and four period 4 islands.

Acknowledgements

C.S. has been supported by grants BFM2003-09504-C02-01, MTM2006-05849/Consolider (Spain) and CIRIT 2005 SGR-1028 (Catalonia). D.T. has been supported by the RFBR grant 05-01-01119 and grant NSh 1312.2006.1. The cluster facilities, HIDRA and EIXAM, of the Dynamical Systems groups at the Univ. de Barcelona and Univ. Politècnica de Catalunya, respectively, have been widely used.

References

[1] Dovbysh S. A., Splitting of separatrices and generation of isolated periodic solutions in Hamiltonian systems with one and a half degrees of freedom, *Uspekhi. Mat. Nauk.*, 1989, Vol. 44, No. 2, 229–230 (in Russian).

[2] Fontich E. and Simó, C., The Splitting of Separatrices for Analytic Diffeomorphisms, *Erg. Th. & Dyn. Systems*, 1990, Vol. 10, 295–318.

[3] Gelfreich V., A proof of the exponentially small transversality of the separatrices for the standard map, *Comm. Math. Phys.*, 1999, Vol. 201, No. 1, 155–216.

[4] Gelfreich, V. and Lazutkin, V., Splitting of separatrices: perturbation theory and exponential smallness, *Russian Math. Surveys*, 2001, Vol. 56, No. 3, 499–558.

[5] Gelfreich V. and Simó, C., High-precision computations of divergent asymptotic series and homoclinic phenomena. This Volume.

[6] Kozlov V. V., Splitting of separatrices and generation of isolated periodic solutions in Hamiltonian systems with one and a half degrees of freedom, *Uspekhi. Mat. Nauk.*, 1986, Vol. 41, No. 5, 177–178 (in Russian).

[7] Moser J. The analytical invariants of an area-preserving mapping near a hyperbolic fixed point. *Commun. Pure and Appl. Math.*, 1956, Vol. 9, No. 4, 673–692.

[8] Simó, C. and Vieiro, A., Some relevant aspects of area preserving maps and the planar conservative Hénon map. Preprint (2006), Univ. Barcelona.

[9] Sinai Ya. G., Several exact results on decay of correlations, in the book: Zaslavsky G.M. Statistical irreversibility in nonlinear systems. [Current Problems in Physics] "Nauka", Moscow 1970 (in Russian).

[10] Treschev D. V., Hyperbolic tori and asymptotic surfaces in Hamiltonian systems, *Russian J. of Math. Phys.*, 1994, Vol. 2, No. 1, 93–110.